Chapter 5

BIFURCATION OF ELASTIC MULTILAYERS

Davide Bigoni, Massimiliano Gei and Sara Roccabianca
Department of Mechanical and Structural Engineering
University of Trento, Via Mesiano 77, I-38123 Trento, Italy

Abstract

The occurrence of a bifurcation during loading of a multilayer sets a limit on structural deformability, and therefore represents an important factor in the design of composites. Since bifurcation is strongly influenced by the contact conditions at the interfaces between the layers, mechanical modelling of these is crucial. The theory of incremental bifurcation is reviewed for elastic multilayers, when these are subject to a finite strain before bifurcation, corresponding to uniform tension/compression and finite bending. The interlaminar contact is described by introducing linear imperfect interfaces. Results are critically discussed in view of applications and available experiments.

5.1 Introduction

Natural (geological formations, biological materials) and man-made (sandwich panels, submarine coatings, microelectronic devices, ceramic capacitors) structures are often made up of layers of different materials glued together, the so-called 'multilayers'. Large strain in these structures is achieved (i) as an industrial need (for instance when forming metallic multilayers [1], 'wrapping' of an engineered tissue around a tubular support to create an artificial blood vessel [2] or bending of multilayer flexible solar cells [3]), (ii) under working conditions (for instance when multilayer films are employed for flexible packaging) or (iii) as a natural process (for instance during morphogenesis of arteries or geological formations or when the leaf of a plant bends to trap an insect, to disperse seeds or to resist dehydration). In all these cases, the occurrence of various forms of bifurcation sets limits to deformation performance. For instance compressive strain is limited

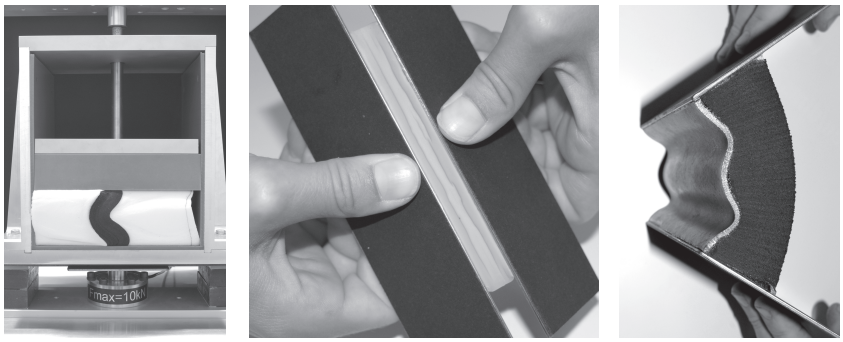

Fig. 5.1. Left: A stiff (30 mm thick, neoprene) layer bonded by two compliant (100 mm thick foam) layers in a rigid-wall, confined compression apparatus (note that separation between sample and wall has occurred on the right upper edge of the sample). Centre: Creases on the compressive side of a rubber strip, coated on the tensile side with a 0.4 mm thick polyester transparent film, subject to flexure. Right: Bifurcation of a two-layer rubber block under finite bending, evidencing long-wavelength bifurcation modes (the stiff layer, made of natural rubber, is on the compressive side of a neoprene block).

by buckling and subsequent folding (see the example Fig. 5.1 on the left-hand side of), uniform tensile strain may terminate with shear band formation and growth, while uniform flexure may lead to the formation of bifurcation modes such as creases and undulations (see the example Fig. 5.1 in the centre and on the right-hand side of). Bifurcation is therefore an important factor in the design of multilayered materials, and so it has been the focus of a thorough research effort, which was initiated by Maurice A. Biot [4] and continued by many others. In particular, elastic layered structures deformed in plane strain and subject to a uniform state of stress have been analysed by Dorris and Nemat-Nasser [5], Steif [6–9], Papamichos, Vardoulakis and Muhlhaus [10], Dowaikh and Ogden [11], Benallal, Billardon and Geymonat [12], Triantafyllidis and Lehner [13], Triantafyllidis and Leroy [14], Shield, Kim and Shield [15], Ogden and Sotiropoulos [16] and Steigmann and Ogden [17] as a bifurcation problem of an isolated layer subject to uniform tension or compression [18–20]. Layered structures subject to finite bending have been considered by Roccabianca, Bigoni and Gei [21,22], who found solutions both for the non-uniform state of stress that develops during flexure[a] and for the related incremental

[a]The solution of finite flexure of an elastic multilayered structure is interesting from different points of view, since the stress state induced by bending is complex (it may involve for instance the presence of more than one neutral axis) and strongly influences bifurcation.

Fig. 5.2. Bifurcation through compression of a finely layered metamorphic rock has induced severe folding. This is an example of a so-called 'accommodation structure' (Trearddur Bay, Holyhead, N. Wales, UK; the coin in the photo is a pound).

bifurcation problem. These findings relied on a generalization of previous results for plane-strain bending of an elastic block given by Rivlin [23] and on analyses of incremental bifurcations [24–30]).

The bifurcation loads and modes are strongly sensitive to the bonding conditions between the layers, which may be perfect (as in the case of the rock shown in Fig. 5.2), but often they may involve the possibility of slip and detachments, the so-called 'delaminations' (as in the cases shown in Fig. 5.3). A simple way to account for this crucial behaviour is to introduce interfacial laws at the contact between layers. The simplest model of these laws is linear and can be formulated by assuming that the interface has null [31–33] or finite [34–36] thickness. We will limit our attention to zero-thickness linear interfaces, across which the nominal traction increment remains continuous, but linearly related to the jump in incremental displacement, which is unrestricted. For simplicity, the materials forming the multilayer are assumed hyperelastic and incompressible, according to the general framework laid by Biot [4], in which Mooney–Rivlin and Ogden materials [37], as well as the J_2-deformation theory of plasticity materials, are particular cases. Therefore, the constitutive laws are broad enough to embrace the behaviour of rubber, plastics, geological materials, but also ductile metals subject to proportional loading, as they can be represented in terms of the J_2-deformation theory.

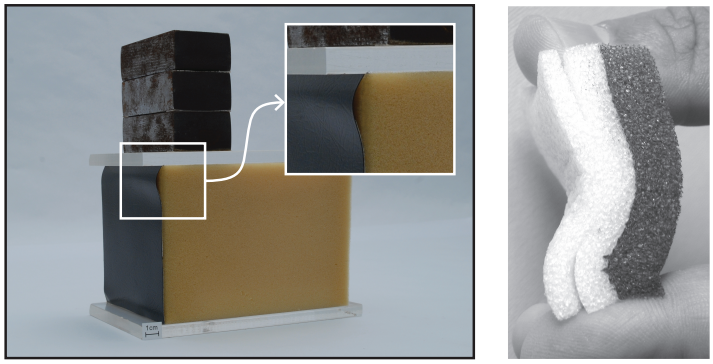

Fig. 5.3. Bifurcation through compression with detachment of layers: Left: A stiff (1 mm thick) plastic coating has detached from the foam substrate to which it was initially glued. Right: Three layers of foam subject to compression show folding with detachment, clearly visible near the edges of the sample.

After the introduction of the constitutive laws for the material and the interfaces (Section 5.2), we start with the problem of an elastic incompressible structure made of straight layers connected through linear interfaces and deformed in a state of uniform biaxial stress, for which incremental bifurcations are sought (Section 5.3). We conclude with the case of finite bending of a layered elastic block, deformed under plane strain (Section 5.4).

5.2 Notations and Governing Equations

The notations employed in this chapter and the main equations governing equilibrium in finite and incremental elasticity are now briefly reviewed. Let $\boldsymbol{x}^0$ denote the position of a material point in some stress-free reference configuration B_0 of an elastic body. A deformation $\boldsymbol{\xi}$ is applied, mapping points of B_0 to those of the current configuration B indicated by $\boldsymbol{x} = \boldsymbol{\xi}(\boldsymbol{x}^0)$. We identify its deformation gradient by $\boldsymbol{F}$, i.e. $\boldsymbol{F} = \mathsf{grad}\boldsymbol{\xi}$, and we define the right $\boldsymbol{C}$ and the left $\boldsymbol{B}$ Cauchy–Green tensors as $\boldsymbol{C} = \boldsymbol{F}^T\boldsymbol{F}$ and $\boldsymbol{B} = \boldsymbol{F}\boldsymbol{F}^T$.

For isotropic incompressible elasticity, the constitutive equations can be written as a relationship between the Cauchy stress $\boldsymbol{T}$ and $\boldsymbol{B}$ as

$$\boldsymbol{T} = -\pi\boldsymbol{I} + \alpha_1\boldsymbol{B} + \alpha_{-1}\boldsymbol{B}^{-1}, \quad \det\boldsymbol{B} = 1, \tag{5.1}$$

where π is an arbitrary Lagrangian multiplier representing hydrostatic pressure and α_1 and α_{-1} are coefficients (such that $\alpha_1 > 0$ and $\alpha_{-1} \leq 0$), which may depend on the deformation.

Alternatively, the principal stresses T_i $(i = 1, 2, 3)$, which are aligned with the Eulerian principal axes, can be obtained in terms of a strain-energy function W, which can be viewed as a function of the principal stretches λ_i $(i = 1, 2, 3)$. For an incompressible material, these relationships take the form (index i not summed)

$$T_i = -\pi + \lambda_i \frac{\partial W(\lambda_1, \lambda_2, \lambda_3)}{\partial \lambda_i}, \quad \lambda_1 \lambda_2 \lambda_3 = 1. \tag{5.2}$$

Equations (5.1) and (5.2) are linked through the following equations [33]

$$\begin{aligned} \alpha_1 &= \frac{1}{\lambda_1^2 - \lambda_2^2} \left[\frac{(T_1 - T_3)\lambda_1^2}{\lambda_1^2 - \lambda_3^2} - \frac{(T_2 - T_3)\lambda_2^2}{\lambda_2^2 - \lambda_3^2} \right], \\ \alpha_{-1} &= \frac{1}{\lambda_1^2 - \lambda_2^2} \left[\frac{T_1 - T_3}{\lambda_1^2 - \lambda_3^2} - \frac{T_2 - T_3}{\lambda_2^2 - \lambda_3^2} \right], \end{aligned} \tag{5.3}$$

which express the coefficients α_1 and α_{-1} in terms of the strain-energy function of the material.

In the absence of body forces, equilibrium is expressed in terms of the first Piola–Kirchhoff stress tensor $\boldsymbol{S} = \boldsymbol{T}\boldsymbol{F}^{-T}$ (note that for incompressible materials $\det \boldsymbol{F} = 1$) as $\mathsf{div}\boldsymbol{S} = \boldsymbol{0}$, an equation defined on B_0.

The loss of uniqueness of plane-strain incremental boundary-value problems is investigated, so that the incremental displacements are given by

$$\boldsymbol{u}(\boldsymbol{x}) = \dot{\boldsymbol{\xi}}(\boldsymbol{x}^0), \tag{5.4}$$

where, as in the following, a superposed dot is used to denote a first-order increment and an updated Lagrangian formulation (where the governing equations are defined in the current configuration B) is adopted. The incremental counterpart of equilibrium is expressed by $\mathsf{div}\boldsymbol{\Sigma} = \boldsymbol{0}$, where the updated incremental first Piola–Kirchhoff stress is given by

$$\boldsymbol{\Sigma} = \dot{\boldsymbol{S}}\boldsymbol{F}^T, \quad \dot{\boldsymbol{S}} = \dot{\boldsymbol{T}}\boldsymbol{F}^{-T} - \boldsymbol{T}\boldsymbol{L}^T\boldsymbol{F}^{-T}. \tag{5.5}$$

The linearized constitutive equation is

$$\boldsymbol{\Sigma} = \mathbb{C}\boldsymbol{L} - \dot{\pi}\boldsymbol{I}, \tag{5.6}$$

where $\boldsymbol{L} = \mathsf{grad}\boldsymbol{u}$ and $\mathbb{C}$ is the fourth-order tensor of instantaneous elastic moduli (possessing the major symmetries). Incompressibility requires that $\mathsf{tr}\boldsymbol{L} = 0$. Since $\boldsymbol{\Sigma} = \dot{\boldsymbol{T}} - \boldsymbol{T}\boldsymbol{L}^T$ (see Eq. (5.5)), the balance of rotational momentum yields $\Sigma_{12} - \Sigma_{21} = T_2 L_{12} - T_1 L_{21}$, and a comparison with Eq. (5.6) shows that (no sum on indices i and j)

$$C_{ijji} + T_i = C_{jiji} \quad (i \neq j). \tag{5.7}$$

For a hyperelastic material, the components of $\mathbb{C}$ can be defined in terms of the strain-energy function W.

For the plane problem addressed here they depend on two incremental moduli [4], namely

$$\mu = \frac{\lambda}{2}\left(\frac{\lambda^4+1}{\lambda^4-1}\frac{d\hat{W}}{d\lambda}\right), \quad \mu_* = \frac{\lambda}{4}\left(\frac{d\hat{W}}{d\lambda} + \lambda\frac{d^2\hat{W}}{d\lambda^2}\right), \tag{5.8}$$

where $\hat{W} = W(\lambda, 1/\lambda, 1)$, due to incompressibility. In the following, examples are given for two specific materials both of which are initially isotropic elastic solids. One is the Mooney–Rivlin material, for which

$$W = \frac{\mu_0}{2}(\lambda_1^2 + \lambda_2^2 - 2), \tag{5.9}$$

where λ_1 and λ_2 are the principal in-plane stretches and μ_0 is the shear modulus in the undeformed configuration. Due to incompressibility $\lambda = \lambda_1$ and $\lambda_2 = 1/\lambda$, so that

$$T_1 = \mu_0(\lambda^2 - \lambda^{-2}) \quad \text{and} \quad \mu = \mu^* = \frac{\mu_0}{2}(\lambda^2 + \lambda^{-2}), \tag{5.10}$$

where the former is the uniaxial tension law (along axis x_1). Notice that the ratio between T_1 and μ is:

$$\frac{T_1}{\mu} = \frac{2(\lambda^2 - \lambda^{-2})}{\lambda^2 + \lambda^{-2}}, \tag{5.11}$$

and its value always ranges between -2 (infinite compression) and 2 (infinite tension). The other material analysed in this section is the J_2-deformation theory solid introduced by Hutchinson and Neale [38], for which

$$W = \frac{K}{N+1}\varepsilon^{N+1}, \quad \mu = \frac{K\varepsilon^N \coth(2\varepsilon)}{2}, \quad \mu^* = \frac{KN\varepsilon^{N-1}}{4}, \tag{5.12}$$

where K is a material parameter, $N \in]0,1]$ is the hardening exponent and ε is the maximum principal logarithmic strain ($\varepsilon = \ln \lambda$). The uniaxial stress-strain law turns out to be $T_1 = K\varepsilon^N$. For this material, the governing equilibrium equations become hyperbolic when [39]

$$\varepsilon_{sb} = \sqrt{N[2\varepsilon_{sb}\coth(2\varepsilon_{sb}) - N]}, \tag{5.13}$$

a threshold which corresponds to the emergence of shear bands in the deformed solid.

At the interfaces between layers we employ the compliant interface model of Suo, Ortiz and Needleman [31] and Bigoni, Ortiz and Needleman [32] for which the jump between incremental stress and incremental displacement can be written, in components (in a reference system with the axis 1 orthogonal to the interface), as

$$\Sigma_{11} = \mathcal{S}_{1m}(u_m^+ - u_m^-), \quad \Sigma_{21} = \mathcal{S}_{2m}(u_m^+ - u_m^-); \tag{5.14}$$

here $\mathcal{S}_{ij}$, the instantaneous stiffness of the interface, is a 2×2 constant matrix whose components have dimension [stress/length]. It is important to notice that the model depends on the situation, as in the present case, in which the stress vector at the interface is null for the fundamental path. The limiting cases of a traction-free and perfectly bonded interface correspond to $\mathcal{S}_{ij} \equiv 0$ and to $\mathcal{S}_{ij} \to \infty$, respectively. $\mathcal{S}_{11}$ represents the normal stiffness and $\mathcal{S}_{22}$ the shear stiffness of the interface. $\mathcal{S}_{12}$ and $\mathcal{S}_{21}$ are the coupling between the normal and shear responses and, in the applications, will be chosen equal to zero. In (5.14), the terms $()^+$ and $()^-$ indicate quantities for the two sides of the interface. In addition to (5.14), continuity of traction across the interface has to be imposed, namely

$$\boldsymbol{\Sigma}^+ \boldsymbol{n} = \boldsymbol{\Sigma}^- \boldsymbol{n}. \tag{5.15}$$

5.3 Uniaxial Tension/Compression of an Elastic Multilayer

In this section bifurcation is analysed for a multilayered elastic structure with straight interfaces separating orthotropic, incompressible layers deformed in plane-strain tension and compression. The fundamental path is characterized by finite, uniform deformations, and the loss of uniqueness in the form of waves of vanishing velocity is considered. The materials in the layers obey a general hyperelastic incompressible constitutive law and specific results are presented for Mooney–Rivlin and J_2-deformation theory materials. Different boundary conditions are imposed at the external

surfaces of the multilayered structure, namely, traction free, and bonding to an elastic or undeformable substrate. The possibility of shear-band instability, due to the loss of ellipticity as seen in the equilibrium equations, is also analysed.

5.3.1 *Equations for a layer*

A laminated structure composed of n-layers is considered, subject to homogeneous large deformation in the fundamental path, so that equilibrium and compatibility are trivially satisfied. Plane-strain conditions are assumed with the principal directions of deformation aligned normal and parallel to the layers (Fig. 5.4), with the additional assumption that each layer, along the fundamental path, is subjected to a uniaxial stress along direction x_2. The possibility of bifurcation from the homogeneous state is investigated by adopting an updated Lagrangian formulation of the field equations where the current configuration is taken as a reference.

The material is a non-linear, orthotropic, incompressible elastic solid and obeys the incremental constitutive equation (5.6). In the absence of body forces, incremental equilibrium requires $\mathrm{div}\,\mathbf{\Sigma} = \mathbf{0}$. In each layer, non-homogeneous incremental solutions are considered in the form

$$u_j = w_j(x_1)e^{ikx_2}(j = 1, 2), \quad \dot{p} = q(x_1)e^{ikx_2}. \tag{5.16}$$

The functions $w_j(x_1)$ and $q(x_1)$ will, in general, differ from layer to layer, but the wave number k is taken to be the same for all layers. A chain substitution of Eq. (5.16) into the constitutive law (5.6) and, finally, into the incremental equilibrium equations yields a system of three constant-coefficient ordinary differential equations for the three unknown functions

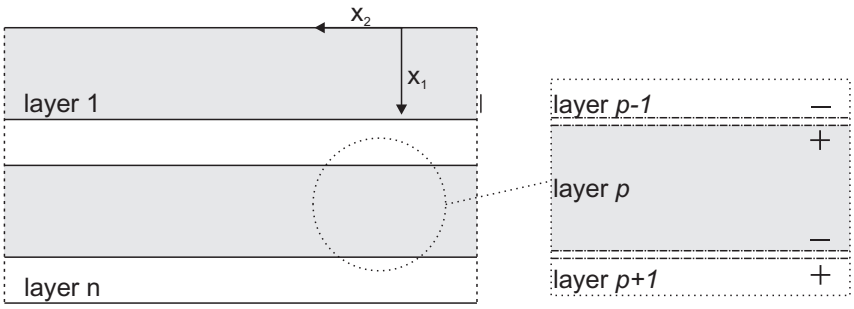

Fig. 5.4. Sketch of the laminated structure. Note that a linear interface is present at each junction between layers.

$w_j(x_1)$ and $q(x_1)$. The solution is

$$\begin{aligned} w_1(x_1) &= b_1 e^{\tau_1 x_1} + b_2 e^{\tau_2 x_1} + b_3 e^{\tau_3 x_1} + b_4 e^{\tau_4 x_1}, \\ w_2(x_1) &= \frac{i}{k}[\tau_1 b_1 e^{\tau_1 x_1} + \tau_2 b_2 e^{\tau_2 x_1} + \tau_3 b_3 e^{\tau_3 x_1} + \tau_4 b_4 e^{\tau_4 x_1}], \\ q(x_1) &= \frac{1}{2}[(C_{2222} - C_{1111} + M)(\tau_1 b_1 e^{\tau_1 x_1} + \tau_2 b_2 e^{\tau_2 x_1}) \\ &\quad + (C_{2222} - C_{1111} - M)(\tau_3 b_3 e^{\tau_3 x_1} + \tau_4 b_4 e^{\tau_4 x_1})], \end{aligned} \tag{5.17}$$

in which $M = \sqrt{L^2 - 4C_{1212}C_{2121}}$ and $L = 2C_{1221} + 2C_{1122} - C_{1111} - C_{2222}$. Coefficients τ_s ($s = 1, \ldots, 4$, $\tau_2 = -\tau_1$, $\tau_4 = -\tau_3$) are the eigenvalues of the equilibrium equations and depend on k, μ, μ^* and T_2. Using the standard classification of regimes, coefficients τ_s may be: (i) real numbers in the elliptic imaginary regime, (ii) two complex conjugate pairs in the elliptic complex regime, (iii) purely imaginary numbers in the hyperbolic regime and (iv) two purely imaginary and two real numbers in the parabolic regime. Departure from the elliptic range corresponds to the occurrence of shear bands. In the following, examples are given for two previously introduced materials, namely, the Mooney–Rivlin and the J_2-deformation theory constitutive models.

Focusing now on the conditions at the interface between layers p and $p+1$ in Fig. 5.4, a substitution of $w_j(x_1)$ and $q(x_1)$ into Eqs. (5.14) and (5.15) yields the interfacial conditions in terms of coefficients b_s^p and $b_s^{(p+1)}$. In matrix form these are

$$\boldsymbol{H}^{p^-}\boldsymbol{b}^p = \boldsymbol{H}^{(p+1)^+}\boldsymbol{b}^{(p+1)}, \tag{5.18}$$

where vectors $\boldsymbol{b}^p$ and $\boldsymbol{b}^{(p+1)}$ collect coefficients b_s for the two layers sharing the interface, while $\boldsymbol{H}^{p^-}$ and $\boldsymbol{H}^{(p+1)^+}$ are the interfacial matrices for layer $-$ and $+$, respectively

$$\boldsymbol{H}^{p^-} = \begin{bmatrix} (e^{\tau x_1}\tau\Gamma)_1^{p^-} & (e^{\tau x_1}\tau\Gamma)_2^{p^-} & (e^{\tau x_1}\tau\Gamma)_3^{p^-} & (e^{\tau x_1}\tau\Gamma)_4^{p^-} \\ (e^{\tau x_1}\Delta)_1^{p^-} & (e^{\tau x_1}\Delta)_2^{p^-} & (e^{\tau x_1}\Delta)_3^{p^-} & (e^{\tau x_1}\Delta)_4^{p^-} \\ (e^{\tau x_1}[\tau\Gamma + \Theta])_1^{p^-} & (e^{\tau x_1}[\tau\Gamma + \Theta])_2^{p^-} & (e^{\tau x_1}[\tau\Gamma + \Theta])_3^{p^-} & (e^{\tau x_1}[\tau\Gamma + \Theta])_4^{p^-} \\ (e^{\tau x_1}[ik\Delta + \Xi])_1^{p^-} & (e^{\tau x_1}[ik\Delta + \Xi])_2^{p^-} & (e^{\tau x_1}[ik\Delta + \Xi])_3^{p^-} & (e^{\tau x_1}[ik\Delta + \Xi])_4^{p^-} \end{bmatrix},$$

$$\boldsymbol{H}^{(p+1)^+} = \begin{bmatrix} (e^{\tau x_1}\tau\Gamma)_1^{(p+1)^+} & (e^{\tau x_1}\tau\Gamma)_2^{(p+1)^+} & (e^{\tau x_1}\tau\Gamma)_3^{(p+1)^+} & (e^{\tau x_1}\tau\Gamma)_4^{(p+1)^+} \\ (e^{\tau x_1}\Delta)_1^{(p+1)^+} & (e^{\tau x_1}\Delta)_2^{(p+1)^+} & (e^{\tau x_1}\Delta)_3^{(p+1)^+} & (e^{\tau x_1}\Delta)_4^{(p+1)^+} \\ (e^{\tau x_1}\Theta)_1^{(p+1)^+} & (e^{\tau x_1}\Theta)_2^{(p+1)^+} & (e^{\tau x_1}\Theta)_3^{(p+1)^+} & (e^{\tau x_1}\Theta)_4^{(p+1)^+} \\ (e^{\tau x_1}\Xi)_1^{(p+1)^+} & (e^{\tau x_1}\Xi)_2^{(p+1)^+} & (e^{\tau x_1}\Xi)_3^{(p+1)^+} & (e^{\tau x_1}\Xi)_4^{(p+1)^+} \end{bmatrix}, \tag{5.19}$$

where the entries in the matrices are

$$\begin{aligned} (e^{\tau x_1}\tau\Gamma)_s^{p^-} &= e^{\tau_s^p x_1^{p^-}}\,\tau_s^p\Gamma_s^p, \quad (e^{\tau x_1}\Delta)_s^{p^-} = e^{\tau_s^p x_1^{p^-}}\,\Delta_s^p, \\ (e^{\tau x_1}[\tau\Gamma+\Theta])_s^{p^-} &= e^{\tau_s^p x_1^{p^-}}\,[\tau_s^p\Gamma_s^p + \Theta_s^{p^-}], \\ (e^{\tau x_1}[ik\Delta+\Xi])_s^{p^-} &= e^{\tau_s^p x_1^{p^-}}\,[ik\Delta_s^p + \Xi_s^{p^-}], \end{aligned} \tag{5.20}$$

and the expressions for Γ_s^p, Δ_s^p, $\Theta_s^{p^-}$ and $\Xi_s^{p^-}$ are, respectively,

$$\begin{aligned} \Gamma_1^p = \Gamma_2^p &= \left[\frac{C_{1111}^p}{2} + \frac{C_{2222}^p}{2} - C_{1122}^p + \frac{M^p}{2}\right], \\ \Gamma_3^p = \Gamma_4^p &= \left[\frac{C_{1111}^p}{2} + \frac{C_{2222}^p}{2} - C_{1122}^p - \frac{M^p}{2}\right], \\ \Delta_s^p &= \left[C_{1221}^p + C_{1212}^p\left(\frac{\tau_s^p}{k}\right)^2\right], \\ \Theta_s^{p^-} &= \mathcal{S}_{11}^{p^-} + i\mathcal{S}_{12}^{p^-}\frac{\tau_s^p}{k}, \quad \Xi_s^{p^-} = \mathcal{S}_{21}^{p^-} + i\mathcal{S}_{22}^{p^-}\frac{\tau_s^p}{k}. \end{aligned} \tag{5.21}$$

Relation (5.18) holds at every interface. To complete the analysis, the boundary conditions at the external surfaces 1^+ and n^- need to be set.

5.3.1.1 *Traction free at the external surface of the multilayer*

With reference to the external surface 1^+ of the multilayer, vanishing of the nominal tractions requires

$$\Sigma_{11}^{1^+} = 0, \quad \Sigma_{21}^{1^+} = 0, \tag{5.22}$$

which can be written in matrix form as

$$\boldsymbol{C}^{1^+}\boldsymbol{b}^1 = \boldsymbol{0},$$

$$\boldsymbol{C}^{1^+} = \begin{bmatrix} (e^{\tau x_1}\tau\Gamma)_1^{1^+} & (e^{\tau x_1}\tau\Gamma)_2^{1^+} & (e^{\tau x_1}\tau\Gamma)_3^{1^+} & (e^{\tau x_1}\tau\Gamma)_4^{1^+} \\ (e^{\tau x_1}\Delta)_1^{1^+} & (e^{\tau x_1}\Delta)_2^{1^+} & (e^{\tau x_1}\Delta)_3^{1^+} & (e^{\tau x_1}\Delta)_4^{1^+} \end{bmatrix}. \tag{5.23}$$

A similar result can be obtained for the free boundary n^-.

5.3.1.2 *Bonding to an elastic half-space at the external surface of the multilayer*

When an elastic half-space is coated with a multilayer, the elastic solution has to decay within it with depth $x_1 \to +\infty$ (or $x_1 \to -\infty$), a condition implying vanishing of the two coefficients b_s corresponding to the eigenvalues τ_s with positive (or negative) real part. Therefore, the interfacial matrices for half-spaces at the upper (label 1) and lower (label n) external surfaces of the multilayer are

$$\begin{aligned} \boldsymbol{H}^{1^-} &= \begin{bmatrix} (e^{\tau x_1}\tau\Gamma)_1^{1^-} & (e^{\tau x_1}\tau\Gamma)_3^{1^-} \\ (e^{\tau x_1}\Delta)_1^{1^-} & (e^{\tau x_1}\Delta)_3^{1^-} \\ (e^{\tau x_1}[\tau\Gamma+\Theta])_1^{1^-} & (e^{\tau x_1}[\tau\Gamma+\Theta])_3^{1^-} \\ (e^{\tau x_1}[ik\Delta+\Xi])_1^{1^-} & (e^{\tau x_1}[ik\Delta+\Xi])_3^{1^-} \end{bmatrix}, \\ \boldsymbol{H}^{(n+1)^+} &= \begin{bmatrix} (e^{\tau x_1}\tau\Gamma)_2^{(n+1)^+} & (e^{\tau x_1}\tau\Gamma)_4^{(n+1)^+} \\ (e^{\tau x_1}\Delta)_2^{(n+1)^+} & (e^{\tau x_1}\Delta)_4^{(n+1)^+} \\ (e^{\tau x_1}\Theta)_2^{(n+1)^+} & (e^{\tau x_1}\Theta)_4^{(n+1)^+} \\ (e^{\tau x_1}\Xi)_2^{(n+1)^+} & (e^{\tau x_1}\Xi)_4^{(n+1)^+} \end{bmatrix}. \end{aligned} \tag{5.24}$$

5.3.1.3 *Bonding to an undeformable substrate at the external surface of the multilayer*

In the case when the external surface of the multilayer is jointed to a smooth undeformable constraint, the normal component of the velocity and the

tangential nominal traction have to vanish. With reference to the surface 1^+ these conditions are

$$v_1^{1^+} = 0, \quad \Sigma_{21}^{1^+} = 0, \tag{5.25}$$

which in matrix form become

$$\begin{aligned} &\boldsymbol{C}^{1^+}\boldsymbol{b}^1 = \boldsymbol{0}, \\ &\boldsymbol{C}^{1^+} = \begin{bmatrix} e^{\tau_1^1 x_1^{1^+}} & e^{\tau_2^1 x_1^{1^+}} & e^{\tau_3^1 x_1^{1^+}} & e^{\tau_4^1 x_1^{1^+}} \\ (e^{\tau x_1}\Delta)_1^{1^+} & (e^{\tau x_1}\Delta)_2^{1^+} & (e^{\tau x_1}\Delta)_3^{1^+} & (e^{\tau x_1}\Delta)_4^{1^+} \end{bmatrix}. \end{aligned} \tag{5.26}$$

5.3.1.4 *Bonding to an undeformable substrate with a compliant interface at the external surface of the multilayer*

In this case, the interfacial constitutive law, Eq. (5.14), is used between the external elastic layer of the multilayer and an undeforming substrate, which behaves as a rigid constraint. At the external surface 1^+, this boundary condition is

$$\begin{aligned} &\boldsymbol{C}^{1^+}\boldsymbol{b}^1 = \boldsymbol{0}, \\ &\boldsymbol{C}^{1^+} = \\ &\begin{bmatrix} (e^{\tau x_1}[\tau\Gamma - \Theta])_1^{1^+} & (e^{\tau x_1}[\tau\Gamma - \Theta])_2^{1^+} & (e^{\tau x_1}[\tau\Gamma - \Theta])_3^{1^+} & (e^{\tau x_1}[\tau\Gamma - \Theta])_4^{1^+} \\ (e^{\tau x_1}[ik\Delta - \Xi])_1^{1^+} & (e^{\tau x_1}[ik\Delta - \Xi])_2^{1^+} & (e^{\tau x_1}[ik\Delta - \Xi])_3^{1^+} & (e^{\tau x_1}[ik\Delta - \Xi])_4^{1^+} \end{bmatrix}, \end{aligned} \tag{5.27}$$

whilst when imposed at the external surface $n-$, it becomes

$$\begin{aligned} &\boldsymbol{C}^{n^-}\boldsymbol{b}^n = \boldsymbol{0}, \\ &\boldsymbol{C}^{n^-} = \\ &\begin{bmatrix} (e^{\tau x_1}[\tau\Gamma + \Theta])_1^{n^-} & (e^{\tau x_1}[\tau\Gamma + \Theta])_2^{n^-} & (e^{\tau x_1}[\tau\Gamma + \Theta])_3^{n^-} & (e^{\tau x_1}[\tau\Gamma + \Theta])_4^{n^-} \\ (e^{\tau x_1}[ik\Delta + \Xi])_1^{n^-} & (e^{\tau x_1}[ik\Delta + \Xi])_2^{n^-} & (e^{\tau x_1}[ik\Delta + \Xi])_3^{n^-} & (e^{\tau x_1}[ik\Delta + \Xi])_4^{n^-} \end{bmatrix}. \end{aligned} \tag{5.28}$$

5.3.2 *Bifurcation criterion*

The set of equations for interfacial and boundary conditions forms a linear system, where the coefficients b_s of all layers are the unknowns. When elastic half-spaces are not present, the dimension of the linear system is $4n \times 4n$. When one elastic half-space or two half-spaces are considered as external

boundary conditions, the order of the linear system becomes $2(2n-1)$ or $4(n-1)$, respectively.

A critical bifurcation condition is attained when a non-trivial solution is possible. This occurs when the system is singular. In terms of interfacial matrices the system can be written as:

$$\begin{bmatrix} \boldsymbol{C}^{1^+} & & : & & 0 \\ \boldsymbol{H}^{1^-} & -\boldsymbol{H}^{2^+} & : & & \\ .. & .. & .. & .. & .. \\ & & : & \boldsymbol{H}^{(n-1)^-} & -\boldsymbol{H}^{n^+} \\ 0 & & : & & -\boldsymbol{C}^{n^-} \end{bmatrix} \begin{bmatrix} \boldsymbol{b}^1 \\ \boldsymbol{b}^2 \\ .. \\ \boldsymbol{b}^{n-1} \\ \boldsymbol{b}^n \end{bmatrix} = \boldsymbol{0} \Rightarrow \boldsymbol{Y}\,\boldsymbol{b} = \boldsymbol{0}, \tag{5.29}$$

and the bifurcation criterion becomes $\det(\boldsymbol{Y}) = \boldsymbol{0}$. The system can be reduced using the transfer matrix method [40,41]. In particular, using the interfacial condition (5.18), the vector $\boldsymbol{b}^p$ can be expressed in terms of $\boldsymbol{b}^{p+1}$ as

$$\boldsymbol{b}^p = (\boldsymbol{H}^{p^-})^{-1}\boldsymbol{H}^{(p+1)^+}\boldsymbol{b}^{p+1}, \tag{5.30}$$

so that, as a consequence, $\boldsymbol{b}^1$ can be given as a function of $\boldsymbol{b}^n$

$$\boldsymbol{b}^1 = \boldsymbol{\Omega}\boldsymbol{b}^n, \quad \boldsymbol{\Omega} = (\boldsymbol{H}^{1^-})^{-1}\boldsymbol{H}^{2^+}(\boldsymbol{H}^{2^-})^{-1}\boldsymbol{H}^{3^+}\ldots(\boldsymbol{H}^{(n-1)^-})^{-1}\boldsymbol{H}^{n^+}, \tag{5.31}$$

where $\boldsymbol{\Omega}$ is the transfer matrix. The linear system is therefore reduced to four equations in four unknowns:

$$\begin{matrix} \boldsymbol{C}^{1^+}\boldsymbol{b}^1 = \boldsymbol{0} \\ \boldsymbol{C}^{n^-}\boldsymbol{b}^n = \boldsymbol{0} \end{matrix} \Rightarrow \begin{matrix} \boldsymbol{C}^{1^+}\boldsymbol{\Omega}\boldsymbol{b}^n = \boldsymbol{0} \\ \boldsymbol{C}^{n^-}\boldsymbol{b}^n = \boldsymbol{0} \end{matrix} \Rightarrow \begin{bmatrix} \boldsymbol{C}^{1^+}\boldsymbol{\Omega} \\ \boldsymbol{C}^{n^-} \end{bmatrix} \boldsymbol{b}^n = \boldsymbol{0} \Rightarrow \boldsymbol{X}\,\boldsymbol{b}^n = \boldsymbol{0}, \tag{5.32}$$

and the bifurcation criterion becomes $\det(\boldsymbol{X}) = \boldsymbol{0}$. Finally notice that, when the number of the layers increases, numerical difficulties due to ill-conditioning may be encountered using the transfer matrix method. An investigation of these problems, well known in the case of infinitesimal elasticity [42–44], would be interesting, but falls beyond the scope of this chapter.

5.3.3 *Results and discussion*

The above described general formulation is applied now to a few simple bifurcation problems. As already remarked, $\mathcal{S}_{12} = \mathcal{S}_{21} = 0$ is assumed. Moreover, the analysis is limited for simplicity to $\mathcal{S}_{11} = \mathcal{S}_{22}$. Results for different interfacial compliances are calculated in terms of the ratio c/h, where h is the thickness of a representative layer and c is given by

$$c = \frac{\mu_1^*}{\mathcal{S}_{11}}, \tag{5.33}$$

where μ_1^* is for layer 1. Parameter c/h is zero for perfect bonding and infinite when the interface becomes a separation surface between two disjointed layers.

In Figs. 5.5 and 5.8, the logarithmic strain ε versus $\bar{k}h$ (where $\bar{k} = k/2\pi$ is the inverse of the wavelength of the bifurcation mode) is shown for a J_2-deformation theory material. Cauchy stress replaces ε in Fig. 5.6 for the Mooney–Rivlin material. A null transversal stress $T_1 = 0$ has been imposed in the fundamental path for all analysed cases. For the J_2-material, loss of ellipticity may occur before bifurcation into a diffuse mode. In particular, condition (5.13) gives $\varepsilon_{sb} = 0.3216$ for $N = 0.1$.

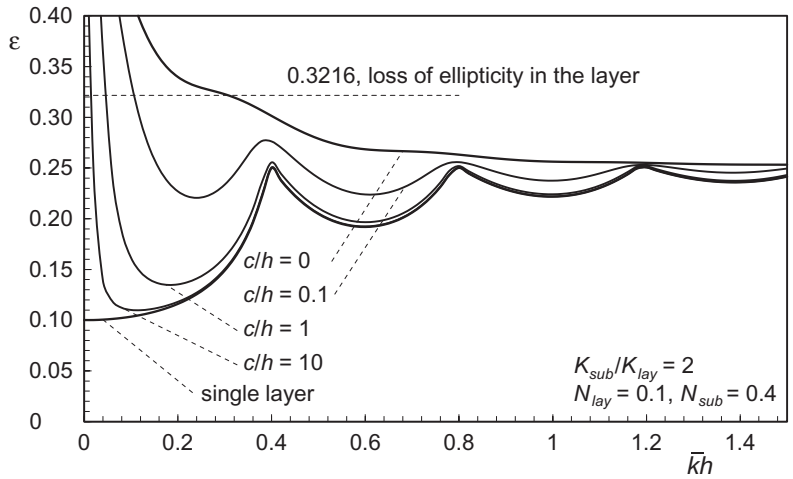

Fig. 5.5. Bifurcation logarithmic strain for a layer bonded to a half-space and loaded under plane-strain uniaxial tension for a J_2-deformation theory material.

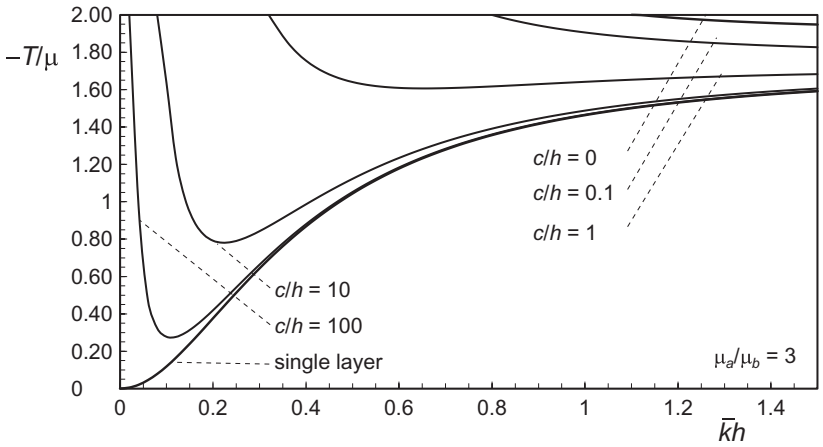

Fig. 5.6. Bifurcation stress for a periodic multilayer in which the representative cell is made of three layers jointed through an imperfect interface and externally bonded to a smooth undeformable substrate. The structure, made of Mooney–Rivlin material, is loaded under plane-strain uniaxial compression.

5.3.3.1 *Layer bonded to a half-space*

The compression case was analysed by Bigoni, Ortiz and Needleman [32] and therefore only the behaviour under tension is investigated here, for a J_2-deformation theory material (Fig. 5.5). The substrate is stiffer than the layer: $K_{sub}/K_{lay} = 2$, $N_{sub} = 0.4$, $N_{lay} = 0.1$. The effect of the interfacial compliance gives a strong reduction in the bifurcation critical strain. In the short wavelength limit ($\bar{k}h \to \infty$) all curves tend to the surface instability value for the layer ($\varepsilon = 0.2524$). For sufficiently large wavelength modes shear bands occur in the layer.

5.3.3.2 *Periodic multilayered structures*

Following [7,13], a periodic multilayered structure can be analysed under certain restrictions as a bifurcation problem of a representative cell (Fig. 5.7), subject to the boundary conditions of contact with smooth undeformable substrates. We consider the layers joined with the imperfect interface defined by Eq. (5.14).

In the example, a ratio $\mu_a/\mu_b = 3$ is assumed for the Mooney–Rivlin material (Fig. 5.6, where T replaces the uniaxial stress T_2). In the case of

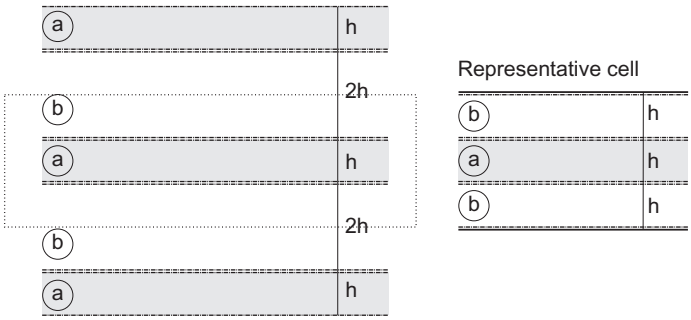

Fig. 5.7. Periodic multilayer structure and representative cell.

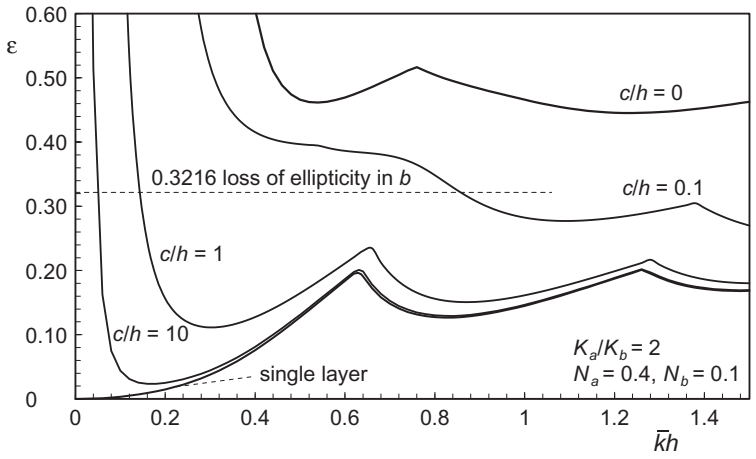

Fig. 5.8. Bifurcation logarithmic strain for a periodic multilayer in which the representative cell is made of three layers jointed through an imperfect interface and externally bonded to a smooth undeformable substrate. The representative cell analysed to model a periodic multilayer is made of J_2-deformation theory material and is loaded under plane-strain uniaxial compression.

perfect bonding, bifurcation is impossible when $\bar{k}h < 1.1$ and the interface instability ($T/\mu = -1.9216$) is approached when $\bar{k}h \to \infty$. When the interfacial compliance increases, the bifurcation load reduces, and the single layer solution [18] is recovered in the limit case of complete separation. The case of compression for J_2-deformation theory material is analysed for the values $K_a/K_b = 2$, $N_a = 0.4$, $N_b = 0.1$ (Fig. 5.8). In all cases, a portion of the curves falls beyond the loss of ellipticity threshold. This portion, in

which homogeneous deformation is terminated by strain localization in the weaker layer, becomes larger as the interface becomes stiffer.

5.4 Bending of Elastic Multilayers with Imperfect Interfaces

In this section we consider elastic multilayers subject to finite flexure, in which the different layers are jointed with imperfect interfaces allowing for full transmission of normal traction and imperfect transmission of shear traction, which are linearly related to a possible jump in the tangential incremental displacement. These conditions are again given by Eqs. (5.14), written now in a cylindrical coordinate system, but with normal stiffness $\mathcal{S}_r \to \infty$. Note that such an interface is not 'activated' during finite bending of a multilayer (since shear tractions are not present at the interfaces between different layers), so that the solution for finite flexure is identical both for perfect and imperfect bonding when $\mathcal{S}_r \to \infty$, but the bifurcation thresholds are strongly affected by the tangential stiffness of the interface $\mathcal{S}_\theta$.

The solution for pure bending of an elastic layered thick plate (of initial 'global' dimensions $l_0 \times h_0$, see Fig. 5.9) made up of N layers jointed through interfaces, which allow complete transmission of normal tractions, follows from an 'appropriate assembling' of solutions relative to the bending of all layers taken separately, a problem analysed by Rivlin [23]. This solution

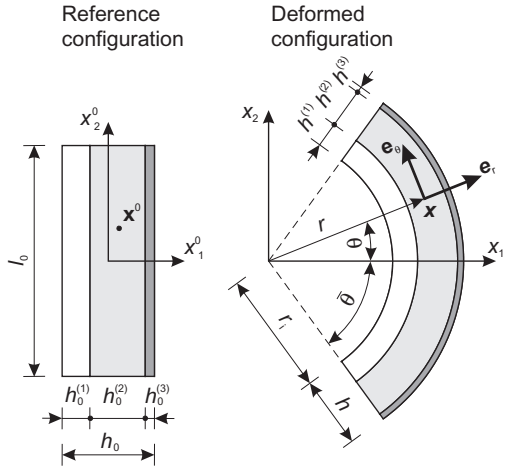

Fig. 5.9. Sketch of a generic layered elastic thick plate subject to finite bending.

is now briefly explained, with reference to a generic layer (the s-th) of the considered multilayer (see [21] for more details).

5.4.1 *Kinematics*

With reference to Fig. 5.9, the generic layer, denoted by the superscript '(s)' ($s = 1, \ldots, N$), is considered in the reference stress-free configuration of a Cartesian coordinate system $O_0^{(s)} x_1^{0(s)} x_2^{0(s)} x_3^{0(s)}$, centred at its centroid, with basis vectors $\boldsymbol{e}_i^0$ ($i = 1, 2, 3$), $x_1^{0(s)} \in [-h_0^{(s)}/2, h_0^{(s)}/2]$, $x_2^{0(s)} \in [-l_0/2, l_0/2]$, and with $x_3^{0(s)}$ denoting the out-of-plane coordinate.

The deformed configuration of each layer is a sector of a cylindrical tube of semi-angle $\bar{\theta}$, which can be referred to as a cylindrical coordinate system $O^{(s)} r^{(s)} \theta^{(s)} z^{(s)}$, with basis vectors $\boldsymbol{e}_r$, $\boldsymbol{e}_\theta$ and $\boldsymbol{e}_z$, $r^{(s)} \in [r_i^{(s)}, r_i^{(s)} + h^{(s)}]$, $\theta^{(s)} \in [-\bar{\theta}, +\bar{\theta}]$, and with out-of-plane coordinate $z^{(s)}$ (Fig. 5.9).

The deformation is prescribed so that a line at constant $x_1^{0(s)}$ transforms to a circular arc at constant $r^{(s)}$, while a line at constant $x_2^{0(s)}$ remains straight but inclined at constant $\theta^{(s)}$. The out-of-plane deformation is null, so that $x_3^{0(s)} = z^{(s)}$. The incompressibility constraint means that

$$r_i^{(s)} = \frac{l_0 h_0^{(s)}}{2\bar{\theta} h^{(s)}} - \frac{h^{(s)}}{2}, \tag{5.34}$$

where $h^{(s)}$ is the current thickness of the circular sector, to be determined. The deformation is described by the functions

$$r^{(s)} = r^{(s)}(x_1^{0(s)}), \quad \theta^{(s)} = \theta^{(s)}(x_2^{0(s)}), \quad z^{(s)} = x_3^{0(s)}, \tag{5.35}$$

so that the deformation gradient takes the form

$$\boldsymbol{F}^{(s)} = \frac{dr^{(s)}}{dx_1^{0(s)}} \boldsymbol{e}_r \otimes \boldsymbol{e}_1^0 + r^{(s)} \frac{d\theta^{(s)}}{dx_2^{0(s)}} \boldsymbol{e}_\theta \otimes \boldsymbol{e}_2^0 + \boldsymbol{e}_z \otimes \boldsymbol{e}_3^0, \tag{5.36}$$

and we can therefore identify the principal stretches as

$$\lambda_r^{(s)} = \frac{dr^{(s)}}{dx_1^{0(s)}}, \quad \lambda_\theta^{(s)} = r^{(s)} \frac{d\theta^{(s)}}{dx_2^{0(s)}} \quad \text{and} \quad \lambda_z^{(s)} = 1. \tag{5.37}$$

Imposition of the incompressibility constraint with Eq. (5.35) yields

$$r^{(s)} = \sqrt{\frac{2}{\alpha^{(s)}} x_1^{0(s)} + \beta^{(s)}}, \quad \theta^{(s)} = \alpha^{(s)} x_2^{0(s)}, \tag{5.38}$$

so that, using Eq. (5.37), the principal stretches can be evaluated as

$$\lambda_r^{(s)} = \frac{1}{\alpha^{(s)} r^{(s)}}, \quad \lambda_\theta^{(s)} = \alpha^{(s)} r^{(s)} \quad \text{and} \quad \lambda_z^{(s)} = 1, \tag{5.39}$$

where $\alpha^{(s)}$ and $\beta^{(s)}$ (Eq. (5.38)) are constants which can be determined by imposing the boundary conditions, which for the s-th layer, are the following:

- At $x_2^{0(s)} = \pm l_0/2$, $\theta^{(s)} = \pm\bar{\theta}$, which from Eq. $(5.38)_2$, $\theta^{(s)} = \pm\alpha^{(s)} l_0/2$, yield

$$\alpha^{(s)} = \frac{2\bar{\theta}}{l_0}, \tag{5.40}$$

  where it is worth noting that $\alpha^{(s)}$ is now independent of the index s;
- At $x_1^{0(s)} = -h_0^{(s)}/2$, $r^{(s)} = r_i^{(s)}$, which from Eqs. (5.34) and $(5.38)_1$, $r_i^{(s)} = r^{(s)}(-h_0^{(s)}/2)$, yield

$$\beta^{(s)} = r_i^{(s)^2} + \frac{l_0 h_0^{(s)}}{2\bar{\theta}}. \tag{5.41}$$

The N layers are assumed to be imperfectly bonded to each other as previously explained, so that continuity of the radial displacements is preserved, and therefore the interfaces do not affect the bending solution. Therefore, we have

$$r_i^{(s)} = r_i^{(s-1)} + h^{(s-1)} \quad (s = 2, \ldots, N), \tag{5.42}$$

with $r_i^{(1)}$ given by $r_i^{(1)} = l_0 h_0^{(1)}/(2\bar{\theta} h^{(1)}) - h^{(1)}/2$ (see Eq. (5.34)). Repeated use of Eqs. (5.34) and (5.42) can be employed to express all thicknesses $h^{(s)}$ $(s = 2, \ldots, N)$ in terms of the thickness of the first layer $h^{(1)}$, which remains the sole kinematical unknown of the problem. In particular, since Eq. (5.42) is imposed at each of the $N - 1$ interfaces between layers, all radial coordinates $r^{(s)}$ share the same origin O of a new cylindrical coordinate system $Or\theta z$, common to all deformed layers (Fig. 5.9 on the right); therefore, the index s on the local current coordinates will be omitted in the following, so that the deformed configuration of the multilayer will be described in terms of the global system $Or\theta z$. From the kinematic analysis, all the stretches are obtained in the multilayer and represented as

$$\lambda_r = \frac{l_0}{2\bar{\theta} r}, \quad \lambda_\theta = \frac{2\bar{\theta} r}{l_0} \quad \text{and} \quad \lambda_z = 1; \tag{5.43}$$

moreover, the current thickness of the s-th layer $h^{(s)}$ becomes a function of $h^{(s-1)}$, namely

$$h^{(s)} = -\frac{l_0 h_0^{(s-1)}}{2\bar{\theta} h^{(s-1)}} - \frac{h^{(s-1)}}{2} + \sqrt{\left(\frac{l_0 h_0^{(s-1)}}{2\bar{\theta} h^{(s-1)}} + \frac{h^{(s-1)}}{2}\right)^2 + \frac{l_0 h_0^{(s)}}{\bar{\theta}}} \quad (s = 2, \ldots, N). \tag{5.44}$$

We may conclude that all current thicknesses are known once the thickness of the first layer $h^{(1)}$ is known (and this will be determined from the solution of the boundary-value problem described in the following section).

5.4.2 *Stress*

Let us analyse now the stress state within the multilayer and consider that the Cauchy stress tensor in a generic layer s can be written as

$$\boldsymbol{T}^{(s)} = T_r^{(s)} \boldsymbol{e}_r \otimes \boldsymbol{e}_r + T_\theta^{(s)} \boldsymbol{e}_\theta \otimes \boldsymbol{e}_\theta + T_z^{(s)} \boldsymbol{e}_z \otimes \boldsymbol{e}_z, \tag{5.45}$$

where, from the constitutive equations (5.2),

$$T_r^{(s)} = -\pi^{(s)} + \lambda_r \frac{\partial W^{(s)}}{\partial \lambda_r}, \quad T_\theta^{(s)} = -\pi^{(s)} + \lambda_\theta \frac{\partial W^{(s)}}{\partial \lambda_\theta}, \tag{5.46}$$

$$T_z^{(s)} = -\pi^{(s)} + \left.\frac{\partial W^{(s)}}{\partial \lambda_z}\right|_{\lambda_z = 1}.$$

Since the stretches only depend on r, the chain rule of differentiation

$$\frac{d\,\cdot}{dr} = \frac{\partial\,\cdot}{\partial \lambda_r}\frac{d\lambda_r}{dr} + \frac{\partial\,\cdot}{\partial \lambda_\theta}\frac{d\lambda_\theta}{dr}, \tag{5.47}$$

together with Eqs. (5.46) and the derivatives of stretches with respect to r (calculated from Eq. (5.39)), can be used in the equilibrium equations

$$\frac{\partial T_r^{(s)}}{\partial r} + \frac{T_r^{(s)} - T_\theta^{(s)}}{r} = 0, \quad \frac{\partial T_\theta^{(s)}}{\partial \theta} = 0, \tag{5.48}$$

to obtain the identities

$$\frac{dW^{(s)}}{dr} = -\frac{T_r^{(s)} - T_\theta^{(s)}}{r} = \frac{dT_r^{(s)}}{dr}. \tag{5.49}$$

Therefore, identifying λ_θ with λ, for a Mooney–Rivlin material (Eq. (5.9)), we arrive at the expressions

$$\begin{aligned} T_r^{(s)} &= \hat{W}^{(s)} + \gamma^{(s)} = \frac{\mu_0^{(s)}}{2}\left(\lambda^2 + \frac{1}{\lambda^2}\right) + \gamma^{(s)}, \\ T_\theta^{(s)} &= \left(\lambda \hat{W}^{(s)}\right)' + \gamma^{(s)} = \frac{\mu_0^{(s)}}{2}\left(3\lambda^2 - \frac{1}{\lambda^2}\right) + \gamma^{(s)}, \end{aligned} \tag{5.50}$$

where $\hat{W}^{(s)}(\lambda) = W^{(s)}(1/\lambda, \lambda, 1)$, $\gamma^{(s)}$ is an integration constant and $()'$ denotes differentiation with respect to the stretch λ. The component $T_z^{(s)}$ can be inferred from Eq. (5.46).

Constants $\gamma^{(s)}$ $(s = 1, \ldots, N)$ and thickness $h^{(1)}$ can be calculated by imposing: (i) continuity of tractions at interfaces between layers ($N - 1$ equations) and (ii) traction-free boundary conditions at the external boundaries of the multilayer (two equations). Considering N layers, the traction continuity at the interfaces is

$$T_r^{(s-1)}(r_i^{(s-1)} + h^{(s-1)}) = T_r^{(s)}(r_i^{(s)}) \quad (s = 2, \ldots, N), \tag{5.51}$$

while null traction at the external surfaces of the multilayer yields

$$T_r^{(1)}(r_i^{(1)}) = 0, \quad T_r^{(N)}(r_i^{(N)} + h^{(N)}) = 0. \tag{5.52}$$

Therefore, $\gamma^{(N)}$ can be calculated from Eq. $(5.52)_2$ and specified for a Mooney–Rivlin strain-energy function as

$$\gamma^{(N)} = -\frac{\mu_0^{(N)}}{2}\left[(\alpha r_e^{(N)})^2 + \frac{1}{(\alpha r_e^{(N)})^2}\right], \tag{5.53}$$

while employing Eq. (5.51), the following recursive formulae are obtained

$$\gamma^{(s-1)} = \frac{\mu_0^{(s)} - \mu_0^{(s-1)}}{2}\left[(\alpha r_e^{(s-1)})^2 + \frac{1}{(\alpha r_e^{(s-1)})^2}\right] + \gamma^{(s)} \quad (s = 2, \ldots, N), \tag{5.54}$$

where $r_i^{(s)} = r_e^{(s-1)}$ (see Eq. (5.42)).

Considering now Eq. $(5.52)_1$ and evaluating $\gamma^{(1)}$ from Eq. (5.54) written for $s = 2$, we obtain an implicit expression to be solved for $h^{(1)}$

$$\frac{\mu_0^{(1)}}{2}\left[(\alpha r_i^{(1)})^2 + \frac{1}{(\alpha r_i^{(1)})^2}\right] + \frac{\mu_0^{(2)} - \mu_0^{(1)}}{2}\left[(\alpha r_e^{(1)})^2 + \frac{1}{(\alpha r_e^{(1)})^2}\right] + \gamma^{(2)} = 0, \tag{5.55}$$

in which $r_i^{(1)}$, $r_e^{(1)}$ and $\gamma^{(2)}$ are all functions of $h^{(1)}$, through Eqs. (5.44) and (5.54).

The obtained solution allows determination of the complex stress and strain fields within a thick, multilayered plate, when subject to finite bending. For instance, we show in Fig. 5.10 the deformed geometries for a four-layer structure (with $l_0/h_0 = 1$, thickness ratios: $h_0^{(b)}/h_0^{(a)} = 2$, $h_0^{(c)}/h_0^{(a)} = 3$ and $h_0^{(d)}/h_0^{(a)} = 4$ and stiffness ratios: $\mu^{(a)}/\mu^{(d)} = 27$, $\mu^{(b)}/\mu^{(d)} = 9$ and $\mu^{(c)}/\mu^{(d)} = 3$), together with graphs of the dimensionless Cauchy principal stresses $T_r(r)/\mu^{(a)}$ (the transverse component) and $T_\theta(r)/\mu^{(a)}$ (the circumferential component).

Note that the transverse stress is always compressive, while the distribution of $T_\theta(r)$ strongly depends on the stiffness of the layer under consideration and always has a null resultant, so that it is equivalent to the bending moment loading the plate. For all cases, the neutral axis (the line corresponding to vanishing circumferential stress) is drawn. Note that in the sketch on the right *two neutral axes* are visible, an interesting feature,

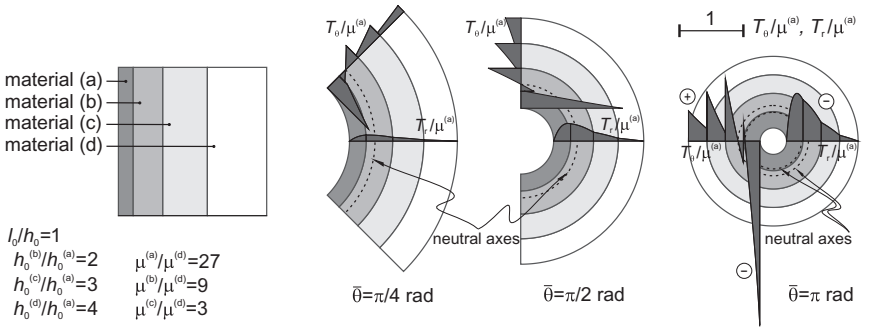

Fig. 5.10. Undeformed and deformed shapes and internal stress states for finite bending of a Mooney–Rivlin four-layer structure with $l_0/h_0 = 1$, thickness ratios: $h_0^{(b)}/h_0^{(a)} = 2$, $h_0^{(c)}/h_0^{(a)} = 3$ and $h_0^{(d)}/h_0^{(a)} = 4$ and stiffness ratios: $\mu^{(a)}/\mu^{(d)} = 27$, $\mu^{(b)}/\mu^{(d)} = 9$ and $\mu^{(c)}/\mu^{(d)} = 3$. Dashed lines represent the neutral axes. Note that two neutral axes are visible in the figure on the right.

which may occur, depending on the geometry and on the properties of layers, for a multilayered plate under finite bending (see [22] for details).

5.4.3 *Incremental bifurcations superimposed on finite bending of an elastic multilayered structure*

We address in this section the plane-strain incremental bifurcation problem of the multilayered thick plate subject to the previously solved (Section 5.4) finite bending deformation. For simplicity we consider the problem of a bilayered structure made of Mooney–Rivlin material, but consideration of additional layers or different constitutive equations is straightforward. The incremental equilibrium is again expressed in terms of the updated incremental first Piola–Kirchhoff stress $\boldsymbol{\Sigma}$ by

$$\mathsf{div}\boldsymbol{\Sigma} = \mathbf{0}, \tag{5.56}$$

where $\boldsymbol{\Sigma}$ is given by Eq. (5.5) in terms of the gradient of incremental displacements $\boldsymbol{L}$, which in cylindrical components can be written as

$$\boldsymbol{L} = u_{r,r}\boldsymbol{e}_r \otimes \boldsymbol{e}_r + \frac{u_{r,\theta} - u_\theta}{r}\boldsymbol{e}_r \otimes \boldsymbol{e}_\theta + u_{\theta,r}\boldsymbol{e}_\theta \otimes \boldsymbol{e}_r + \frac{u_r + u_{\theta,\theta}}{r}\boldsymbol{e}_\theta \otimes \boldsymbol{e}_\theta, \tag{5.57}$$

and is subject to the constraint $\mathsf{tr}\boldsymbol{L} = 0$ (incremental incompressibility), namely,

$$ru_{r,r} + u_r + u_{\theta,\theta} = 0. \tag{5.58}$$

The linearized constitutive equation is given by Eq. (5.6) and for a Mooney–Rivlin material, the components of $\mathbb{C}$ can be written as functions of two incremental moduli, denoted by μ and μ_*, Eq. (5.10), and depending on the value of the current strain. In cylindrical coordinates, the non-vanishing components of $\mathbb{C}$ are [18,45]

$$\begin{aligned} &C_{rrrr} = C_{\theta\theta\theta\theta} = 2\mu_* + p, \quad C_{\theta r\theta r} = \mu - \Gamma, \\ &C_{r\theta r\theta} = \mu + \Gamma, \qquad\qquad C_{r\theta\theta r} = C_{\theta rr\theta} = \mu + p, \end{aligned} \tag{5.59}$$

where Γ and p are given by

$$\Gamma = \frac{T_\theta - T_r}{2}, \quad \text{and} \quad p = -\frac{T_\theta + T_r}{2}, \tag{5.60}$$

describing the state of prestress. Therefore, the incremental constitutive equations (5.6) take, for each layer, the explicit form

$$\begin{aligned}
\Sigma_{rr} &= -\dot{\pi} + (2\mu_* + p)u_{r,r},\\
\Sigma_{\theta\theta} &= -\dot{\pi} + (2\mu_* + p)\frac{u_r + u_{\theta,\theta}}{r},\\
\Sigma_{r\theta} &= (\mu + \Gamma)\frac{u_{r,\theta} - u_\theta}{r} + (\mu + p)u_{\theta,r},\\
\Sigma_{\theta r} &= (\mu + p)\frac{u_{r,\theta} - u_\theta}{r} + (\mu - \Gamma)u_{\theta,r}.
\end{aligned} \tag{5.61}$$

We seek bifurcations represented by an incremental displacement field in the form

$$\begin{cases}
u_r(r,\theta) = f(r)\cos n\theta,\\
u_\theta(r,\theta) = g(r)\sin n\theta,\\
\dot{\pi}(r,\theta) = k(r)\cos n\theta,
\end{cases} \tag{5.62}$$

so that Eq. (5.58) can be reformulated as

$$g = -\frac{(f + rf')}{n}, \tag{5.63}$$

and the incremental equilibrium equations as

$$\begin{aligned}
k' &= Df'' + \left(C_{,r} + D_{,r} + \frac{C + 2D}{r}\right)f' + \frac{E(1 - n^2)}{r^2}f,\\
k &= \frac{r^2 C}{n^2}f''' + \frac{F + 3C}{n^2}rf'' + \left(\frac{F}{n^2} - D\right)f' - \frac{1 - n^2}{n^2}\frac{F}{r}f,
\end{aligned} \tag{5.64}$$

where coefficients C, D, E and F can be expressed (for a Mooney–Rivlin material) as

$$\begin{aligned}
&C = \mu - \Gamma = \frac{\mu_0}{\lambda^2}, \qquad D = 2\mu_* - \mu = \frac{\mu_0}{2}\frac{\lambda^4 + 1}{\lambda^2},\\
&E = \mu + \Gamma = \mu_0\lambda^2, \quad F = rC_{,r} + C = -\frac{\mu_0}{\lambda^2}.
\end{aligned} \tag{5.65}$$

By differentiating Eq. $(5.64)_2$ with respect to r and substituting the result into Eq. $(5.64)_1$, a single differential equation in terms of $f(r)$ is

obtained

$$\begin{aligned} &r^4 f'''' + 2r^3 f''' - (3 + n^2(\lambda^4 + 1))r^2 f'' \\ &+(3 + n^2(1 - 3\lambda^4))r f' + (n^2 - 1)(3 + n^2\lambda^4) f = 0, \end{aligned} \tag{5.66}$$

defining the function $f(r)$ within a generic layer. Once $f(r)$ is known for each layer, the other functions, $g(r)$ and $k(r)$, can be calculated by employing Eqs. (5.63) and $(5.64)_2$, respectively, so that function $f(r)$ becomes the primary unknown.

The differential Eq. (5.66) for the functions $f^{(s)}(r)$ $(s = 1, \ldots, N)$ is complemented by the following boundary conditions:

- Continuity of incremental tractions at interfaces:

$$\Sigma_{rr}^{(s)}\Big|_{r=r_e^{(s)}} = \Sigma_{rr}^{(s+1)}\Big|_{r=r_i^{(s+1)}}, \quad \Sigma_{\theta r}^{(s)}\Big|_{r=r_e^{(s)}} = \Sigma_{\theta r}^{(s+1)}\Big|_{r=r_i^{(s+1)}}; \tag{5.67}$$

- Continuity of the radial component of the incremental displacement at the interfaces:

$$u_r^{(s)}\Big|_{r=r_e^{(s)}} = u_r^{(s+1)}\Big|_{r=r_i^{(s+1)}}; \tag{5.68}$$

- Imperfect 'shear-type' interface (obtained from Eq. (5.14) taking $\mathcal{S}_r \to \infty$)

$$\Sigma_{\theta r}^{(s)}\Big|_{r=r_e^{(s)}} = \mathcal{S}_\theta \left(u_\theta^{(s+1)^+} - u_\theta^{(s)^-}\right), \tag{5.69}$$

  where $\mathcal{S}_\theta$ is a positive shear stiffness coefficient, so that perfect bonding is recovered in the limit $\mathcal{S}_\theta \to \infty$;
- For dead-load tractions on the external surfaces, the boundary conditions at $r = r_i^{(1)}$ and $r = r_e^{(N)}$ are

$$\Sigma_{rr}^{(1),(N)}\Big|_{r=r_i^{(1)}, r_e^{(N)}} = 0, \quad \Sigma_{\theta r}^{(1),(N)}\Big|_{r=r_i^{(1)}, r_e^{(N)}} = 0. \tag{5.70}$$

On the boundaries $\theta = \pm\bar{\theta}$ we require that shear stresses and incremental normal displacements vanish

$$\Sigma_{r\theta}^{(s)}\Big|_{\theta=\pm\bar{\theta}} = 0, \quad u_\theta^{(s)}\Big|_{\theta=\pm\bar{\theta}} = 0, \tag{5.71}$$

a condition which is achieved if $\sin n\bar{\theta} = 0$ (see Eq. (5.62)) or equivalently using Eq. (5.40), if

$$n = \frac{2m\pi}{\alpha l_0} \quad (m \in \mathbb{N}). \tag{5.72}$$

5.4.4 *An example: bifurcation of a bilayer*

The critical angle $\bar{\theta}_{cr}$ and the critical stretch λ_{cr} (on the compressive side of the specimen) for a bilayer at bifurcation are shown in Fig. 5.11 as functions of the aspect ratio l_0/h_0 (the unloaded height of the specimen is l_0 and global thickness is h_0, see Fig. 5.9), for the thickness and stiffness ratios $h_0^{(lay)}/h_0^{(coat)} = 10$ and $\mu^{(coat)}/\mu^{(lay)} = 20$, respectively. In the figure, bifurcation curves are shown for different values of the integer parameter m which, through Eq. (5.72), defines the circumferential wave number n. Obviously, for a given value of l_0/h_0 the bifurcation threshold is set by the value of m providing the minimum (or maximum) value of the critical angle (or stretch).

In the same figure, the threshold for surface instability of the 'soft' layer material ($\lambda_{\text{surf}} \approx 0.545$ [4]) is also shown. It can be deduced from the figure that a diffuse mode, which set the bifurcation thresholds, always exists before surface instability for each aspect ratio l_0/h_0. It is important to observe that the occurrence of the critical diffuse mode is very close to the surface instability when the coating is located on the tensile side of the specimen (Fig. 5.11). The critical angle at bifurcation is given in Fig. 5.12 as a function of the aspect ratio l_0/h_0, for two values of the coating thickness, $h_0^{(lay)}/h_0^{(coat)} = \{10, 20\}$, and when the coating layer is on the tensile side. In the same figure, results for the uncoated layer are also shown for comparison.

It is evident from the figures that the bifurcation solution for a single layer is approximated by a straight line, so that we can define an approximate solution

$$\bar{\theta}_{cr} = 0.712\, l_0/h_0, \tag{5.73}$$

which is very useful for applications. We may also notice that a linear relation between $\bar{\theta}_{cr}$ and l_0/h_0 is found for the bilayer (Figs. 5.11, 5.12 and 5.16); however, the inclination of such lines depends on the elastic and thickness contrasts between the layer and coating, so that it is difficult to obtain a simple formula like Eq. (5.73) in this case.

The effects of an imperfect interface on bifurcations of a layered block under bending have never been analysed, so we limit the discussion to a

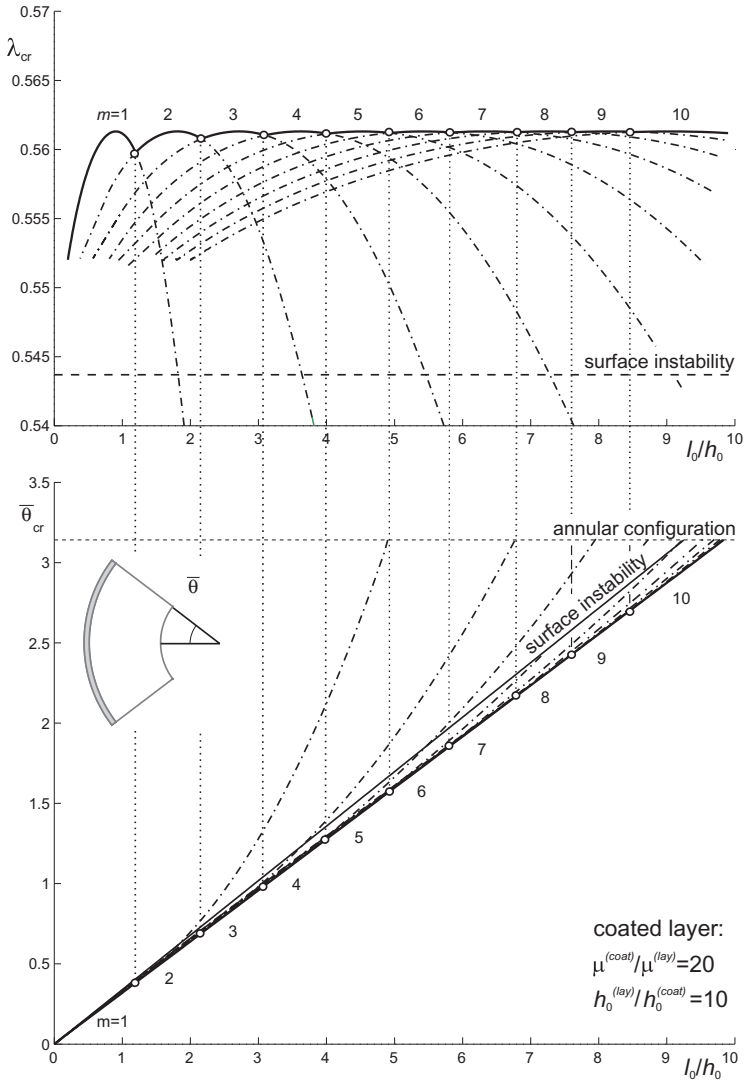

Fig. 5.11. Critical angle $\bar{\theta}_{cr}$ and critical stretch λ_{cr} (evaluated at the internal boundary, $r = r_i^{(1)}$) versus aspect ratio l_0/h_0 of a Mooney–Rivlin coated bilayer subject to bending with $h_0^{(lay)}/h_0^{(coat)} = 10$ and $\mu^{(coat)}/\mu^{(lay)} = 20$. The coating is located on the tensile side of the structure. In both plots, a small circle denotes a transition between two different integer values of m (the parameter which sets the circumferential wave number).

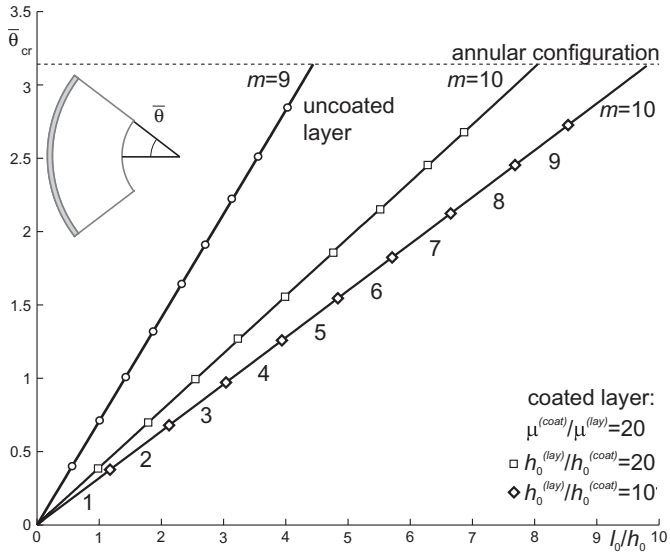

Fig. 5.12. Comparison between the critical angle $\bar{\theta}_{cr}$ at bifurcation versus aspect ratio l_0/h_0 of two Mooney–Rivlin coated bilayers subject to bending with the coating on the tensile side of the structure, with $\mu^{(coat)}/\mu^{(lay)} = 20$ and $h_0^{(lay)}/h_0^{(coat)} = 10$ and 20, respectively. On each curve, a small symbol denotes a transition between two different integer values of m (the parameter which sets the circumferential wave number). Bifurcation angles for a single, uncoated layer are also shown.

simple situation, while a more detailed presentation will be the subject of future research. The simple example analysed in Figs. 5.13 and 5.14 pertains to a uniform elastic block divided into two identical layers through an imperfect interface of stiffness $\mathcal{S}_\theta$ and $\mathcal{S}_r \to \infty$. Results presented in Figs. 5.13 and 5.14 are in terms of the critical bending angle for bifurcation $\bar{\theta}_{cr}$ versus the initial 'global' aspect ratio l_0/h_0, as a function of the dimensionless interfacial stiffness parameter $\mathcal{S}_\theta h_0/\mu_0$. Results for several values of this parameter (ranging between 0 and 1000) are shown in Fig. 5.13, while those results for only two (namely, 0 and 10) are shown in Fig. 5.14.

Only the smallest circumferential number $m = 1$ was considered for Fig. 5.13, so that $\bar{\theta}$ is not always 'critical', since for low values of the aspect ratio l_0/h_0 the onset of instability is associated with higher values of m.

A general conclusion that can be drawn from the results shown in Figs. 5.13 and 5.14 is that the bifurcation threshold strongly depends on the dimensionless parameter $\mathcal{S}_\theta h_0/\mu_0$, which yields an important decrease in

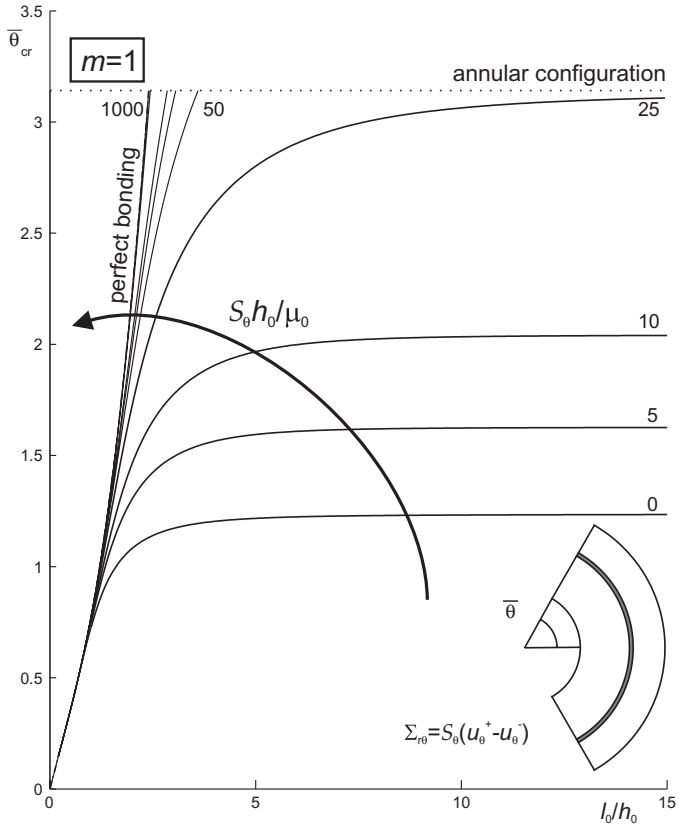

Fig. 5.13. Critical angle $\bar{\theta}_{cr}$ at bifurcation ($m = 1$) versus the 'global' aspect ratio l_0/h_0 for two Mooney–Rivlin identical layers subjected to flexure and jointed through a 'shear-type' imperfect interface of dimensionless stiffness $\mathcal{S}_\theta h_0/\mu_0$. Perfect bonding corresponds to $\mathcal{S}_\theta h_0/\mu_0 \to \infty$.

the bifurcation angles with respect to the perfectly bonded case, approached when $\mathcal{S}_\theta h_0/\mu_0 \to \infty$.

5.4.5 *Experiments on coated and uncoated rubber blocks under bending*

To substantiate the theoretical results for the bifurcation of layered structures subject to finite bending, Roccabianca, Bigoni and Gei [21,22] designed and performed experiments, similar to those initiated by Gent and Cho [46,47]. In these experiments, a finite flexure was imposed on

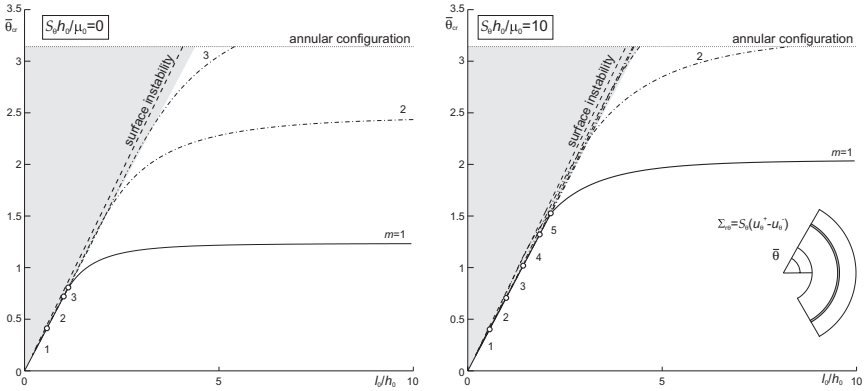

Fig. 5.14. Bifurcation angles $\bar{\theta}_{cr}$ versus the 'global' aspect ratio l_0/h_0 for two Mooney–Rivlin identical layers subjected to flexure and jointed through a 'shear-type' imperfect interface as in Fig. 5.13. Left: $\mathcal{S}_\theta h_0/\mu_0 = 0$; right: $\mathcal{S}_\theta h_0/\mu_0 = 10$. The small numbers near a curve denote the value of the circumferential number m. The lower boundary of the grey region is the bifurcation threshold for perfect bonding.

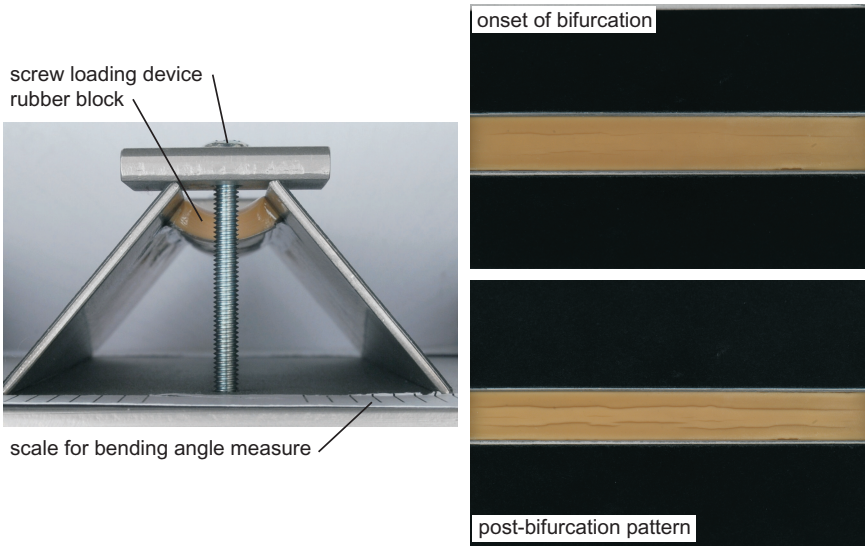

Fig. 5.15. Left: Device used to impose a finite bending (of semi-angle $\bar{\theta}$ equal to 35° in the photo). Right: Bifurcation of a $20 \times 4 \times 100\,\text{mm}^3$ rubber block, coated with two polyester 0.2 mm thick films on the tensile side. Top: Onset of bifurcation ($\bar{\theta} = 40°$, creases become visible). Lower: Post-bifurcation pattern ($\bar{\theta} = 50°$, creases invade the whole specimen).

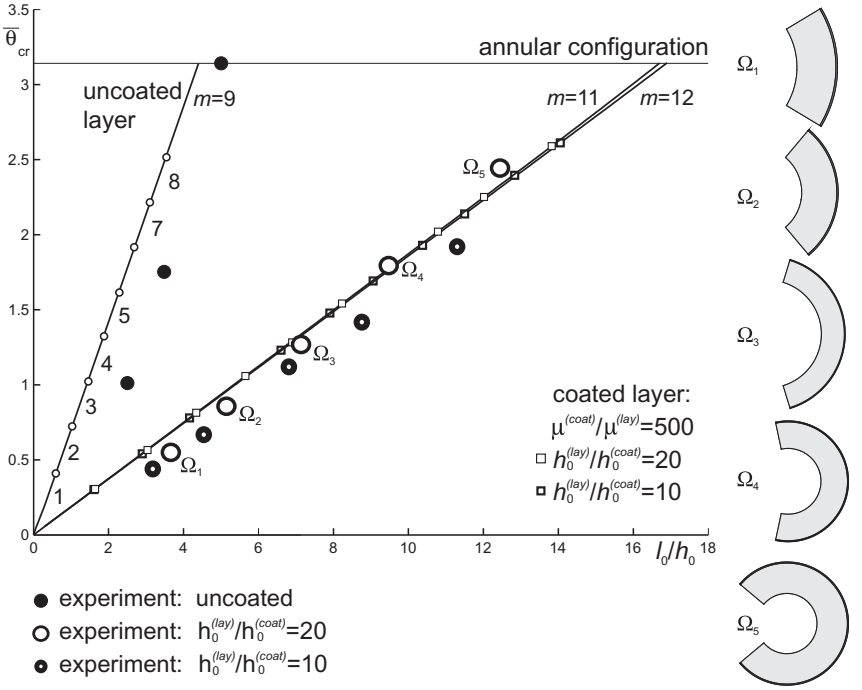

Fig. 5.16. Experimental results versus theoretical predictions for the bifurcation opening semi-angle $\bar{\theta}_{cr}$ of uncoated and coated rubber strips subject to finite bending, versus the aspect ratio l_0/h_0 of the undeformed configuration. The shear moduli ratio $\mu^{(coat)}/\mu^{(lay)}$ of the coated layers has been taken equal to 500, while two thickness ratios $h_0^{(lay)}/h_0^{(coat)}$ equal to 20 and 10 were considered. The critical theoretical configurations (for $h_0^{(lay)}/h_0^{(coat)} = 20$) corresponding to bifurcation points Ω_i $(i = 1, \ldots, 5)$ are sketched the right on the figure.

uncoated and coated elastic blocks (made of natural rubber), glued to two metallic platelets, which were forced to bend by a simple screw loading device (Fig. 5.15 left; see also [21]).

Different coatings and blocks were tested. Bending results for three uncoated rubber strips (made of natural rubber with a ground-state shear modulus $\mu^{(\mathrm{lay})} \cong 1\,\mathrm{N/mm^2}$) and ten coated strips of the same dimensions with two types of coating (both made of a polyester transparent film having $\mu^{(\mathrm{coat})} \cong 500\,\mathrm{N/mm^2}$ but with different thicknesses), all situated on the tensile side of the structure, are shown in Fig. 5.16. At a certain stage of finite bending, namely at a certain bending semi-angle $\bar{\theta}_{cr}$, creases can be detected on the surface of the sample, as in Fig. 5.15

on the right (and in Fig. 5.1 in the centre). This has been identified with the appearance of small wavelength bifurcations and compared with theoretical predictions for uncoated layers and for a layer with a stiff coating on the tensile side of the specimen, in terms of the critical bending semi-angle ($\bar{\theta}_{cr}$) at bifurcation versus the aspect ratio of the samples, Fig. 5.16. Experiments demonstrate that the trend predicted by the theory is qualitatively very well followed, while quantitatively experimental values for bifurcation angles are often a bit lower than the theoretical predictions, a result consistent with observations by Gent and Cho [46]. The fact that experimental results substantiate theoretical predictions allows us to conclude that bifurcation theory can be successfully employed to predict the deformational capabilities of a composite plate subject to finite bending.

In the case when the coating is applied to the compressed side, long wavelengths become visible in the experiment, as qualitatively demonstrated in Fig. 5.1 on the right (see also [22]), while quantitative evaluation still requires further investigation.

5.5 Conclusions

The load-carrying capacity of laminated structures is often limited by the occurrence of various instabilities at different structural levels. Among these, delamination is the best known. Accordingly, there is a large literature where bifurcations and instabilities of multilayers are analysed from a variety of perspectives.

We have shown that the theory of incremental bifurcation of prestressed elastic solids, in which each layer is treated as an elastic non-linear continuum and plate-like approximations are not introduced, can be effectively used to find threshold loads for delamination involving complex bifurcation modes. The presented framework is broad enough to include several constitutive laws modelling the mechanical response of (i) the interfaces (for instance spring-like or shear-type junctions) and (ii) the layers (for instance Mooney–Rivlin and J_2-deformation theory of plasticity materials).

The bifurcation analysis, carried out for different deformation paths including finite tension/compression of straight layers and finite bending, reveals a number of different instabilities that may occur in a multilayer, including Euler buckling, necking, surface instability and various wave-like

modes. The occurrence of one or another form of instability is strongly related to the interfacial conditions between the layers.

Acknowledgements

D.B. gratefully acknowledges the support from the European Union Seventh Framework Programme under contract no. PIAP-GA-2011-286110-INTERCER2. M.G. and S.R. gratefully acknowledge the support of Italian Ministry of Education, University and Research under PRIN grant no. 2009XWLFKW, "Multi-scale modelling of materials and structures".

References

[1] Yanagimoto J., Oya T., Kawanishi S., Tiesler N., Koseki T., 2010. Enhancement of bending formability of brittle sheet metal in multilayer metallic sheets, *CIRP Annals Manufacturing Tech.*, 59, 287–290.
[2] L'Heureux N., Dusserre N., Konig G., Victor B., Keire P., *et al.*, 2006. Human tissue-engineered blood vessel for adult arterial revascularization, *Nature Medicine*, 12, 361–365.
[3] Fan Z., Razavi H., Do J., Morikawi A., *et al.*, 2009. Three-dimensional nanopillar-array photovoltaics on low-cost and flexible substrates, *Nature Materials*, 8, 648–653.
[4] Biot M.A., 1965. *Mechanics of Incremental Deformations*, Wiley, New York.
[5] Dorris J.F., Nemat-Nasser S., 1980. Instability of a layer on a half space, *J. Appl. Mech.*, 47, 304–312.
[6] Steif P.S., 1986. Bimaterial interface instabilities in plastic solids, *Int. J. Solids Struct.*, 22, 195–207.
[7] Steif P.S., 1986. Periodic necking instabilities in layered plastic solids, *Int. J. Solids Struct.*, 22, 1571–1578.
[8] Steif P.S., 1987. An exact two-dimensional approach to fiber microbuckling, *Int. J. Solids Struct.*, 23, 1235–1246.
[9] Steif P.S., 1990. Interfacial instabilities in an unbounded layered solid, *Int. J. Solids Struct.*, 26, 915–925.
[10] Papamichos E., Vardoulakis I., Muhlhaus H.B., 1990. Buckling of layered elastic media: A Cosserat-continuum approach and its validation, *Int. J. Numer. Anal. Meth. Geomech.*, 14, 473–498.
[11] Dowaikh M.A., Ogden R.W., 1991. Interfacial waves and deformations in pre-stressed elastic media, *Proc. R. Soc. Lond. A*, 443, 313–328.
[12] Benallal A., Billardon R., Geymonat G., 1993. Bifurcation and localization in rate-independent materials: Some general considerations, in *CISM Lecture Notes No. 327*, Springer, Berlin, pp. 1–47.
[13] Triantafyllidis N., Lehner F.K., 1993. Interfacial instability of density-stratified 2–layer systems under initial stress, *J. Mech. Phys. Solids*, 41, 117–142.

[14] Triantafyllidis N., Leroy Y.M., 1994. Stability of a frictional material layer resting on a viscous half-space, *J. Mech. Phys. Solids*, 42, 51–110.
[15] Shield T.W., Kim K.S., Shield R.T., 1994. The buckling of an elastic layer bonded to an elastic substrate in plane strain, *J. Appl. Mech.*, 61, 231–235.
[16] Ogden R.W., Sotiropoulos D.A., 1995. On interfacial waves in prestressed layered incompressible elastic solid, *Proc. R. Soc. Lond. A*, 450, 319–341.
[17] Steigmann D.J., Ogden R.W., 1997. Plane deformations of elastic solids with intrinsic boundary elasticity, *Proc. R. Soc. Lond. A*, 453, 853–877.
[18] Hill R., Hutchinson J.W., 1975. Bifurcation phenomena in the plane tension test, *J. Mech. Phys. Solids*, 23, 239–264.
[19] Young N.J.B., 1976. Bifurcation phenomena in the plane compression test, *J. Mech. Phys. Solids*, 24, 77–91.
[20] Needleman A., 1979. Non-normality and bifurcation in plane strain tension or compression, *J. Mech. Phys. Solids*, 27, 231–254.
[21] Roccabianca S., Gei M., Bigoni D., 2010. Plane strain bifurcations of elastic layered structures subject to finite bending: Theory versus experiments, *IMA J. Appl. Math.*, 75, 525–548.
[22] Roccabianca S., Bigoni D., Gei M., 2011. Long wavelength bifurcations and multiple neutral axes of elastic layered structures subject to finite bending, *J. Mech. Mat. Struct.*, 6, 511–527.
[23] Rivlin R.S., 1949. Large elastic deformations of isotropic materials. V. The problem of flexure, *Proc. R. Soc. Lond. A*, 195, 463–473.
[24] Triantafyllidis N., 1980. Bifurcation phenomena in pure bending, *J. Mech. Phys. Solids*, 28, 221–245.
[25] Aron M., Wang Y., 1995. Remarks concerning the flexure of a compressible nonlinearly elastic rectangular block, *J. Elasticity*, 40, 99–106.
[26] Aron M., Wang Y., 1995. On deformations with constant modified stretches describing the bending of rectangular blocks, *Quart. J. Mech. Appl. Math.*, 48, 375–387.
[27] Dryburgh G., Ogden R.W., 1999. Bifurcation of an elastic surface-coated incompressible isotropic elastic block subject to bending, *Z. Angew. Math. Phys.*, 50, 822–838.
[28] Bruhns O., Xiao H., Meyers A., 2002. Finite bending of a rectangular block of an elastic Hencky material, *J. Elasticity*, 66, 237–256.
[29] Bruhns O., Gupta N.K., Meyers A.T.M., Xiao H., 2003. Bending of an elastoplastic strip with isotropic and kinematic hardening, *Arch. Appl. Mech.*, 72, 759–778.
[30] Coman C.D., Destrade M., 2008. Asymptotic results for bifurcation in pure bending of rubber blocks, *Quart. J. Mech. Appl. Math.*, 61, 395–414.
[31] Suo Z., Ortiz M., Needleman A., 1992. Stability of solids with interfaces, *J. Mech. Phys. Solids*, 40, 613–640.
[32] Bigoni D., Ortiz M., Needleman A., 1997. Effect of interfacial compliance on bifurcation of a layer bonded to a substrate, *Int. J. Solids Struct.*, 34, 4305–4326.

[33] Bigoni D., Gei M., 2001. Bifurcations of a coated, elastic cylinder, *Int. J. Solids Struct.*, 38, 5117–5148.
[34] Bigoni D., Movchan A.B., 2002. Statics and dynamics of structural interfaces in elasticity, *Int. J. Solids Struct.*, 39, 4843–4865.
[35] Bertoldi K., Bigoni D., Drugan W.J., 2007. Structural interfaces in linear elasticity. Part I: Nonlocality and gradient approximations, *J. Mech. Phys. Solids*, 55, 1–34.
[36] Brun M., Guenneau S., Movchan A.B., Bigoni D., 2010. Dynamics of structural interfaces: Filtering and focussing effects for elastic waves, *J. Mech. Phys. Solids*, 58, 1212–1224.
[37] Ogden R.W., 1982. Elastic deformations of rubberlike solids, in *Mechanics of Solids*, *The Rodney Hill, 60th Anniversary Volume* (H.G. Hopkins, M.J. Sewell, eds), Pergamon Press, Oxford, pp. 499–537.
[38] Hutchinson J.W., Neale K.W., 1979. Finite strain J_2-deformation theory, *Proc. IUTAM Symp. on Finite Elasticity* (D.E. Carlson, R.T. Shield, eds), Martinus Nijhoff, The Hague, Boston, London, pp. 237–247.
[39] Hutchinson J.W., Tvergaard V., 1981. Shear band formation in plane strain, *Int. J. Solids Struct.*, 17, 451–470.
[40] Thomson W.T., 1950. Transmission of elastic waves through a stratified solid medium, *J. Appl. Mech.*, 21, 89–93.
[41] Bufler H., 1965. Die Druckstabilitt rechteckiger Verbundplatten, *Ingenieur Archiv*, 31, 109–128.
[42] Pilkey W.D., 1993. *Formulas for Stress, Strain, and Structural Matrices*, John Wiley and Sons, New York.
[43] Su X.Y., Tian J.Y., Pao Y-H., 2002. Application of the reverberation-ray matrix to the propagation of elastic waves in a layered solid, *Int. J. Solids Struct.*, 39, 5447–5463.
[44] Tian J.Y., Yang W.X., Su X.Y., 2006. Transient elastic waves in a transversely isotropic laminate impacted by axisymmetric load, *J. Sound Vibr.*, 289, 94–108.
[45] Gei M., Ogden R.W., 2002. Vibration of a surface-coated elastic block subject to bending, *Math. Mech. Solids*, 7, 607–628.
[46] Gent A.N., Cho I.S., 1999. Surface instabilities in compressed or bent rubber blocks, *Rubber Chem. Technol.*, 72, 253–262.
[47] Gent A.N., 2005. Elastic instabilities in rubber, *Int. J. Non-linear Mech.*, 40, 165–175.